

RIBES

Radial basis functions at fluid Interface Boundaries to Envelope flow results for advanced Structural analysis

RIBES test article design

November 2016



Project coordinator:

Prof. Marco Evangelos Biancolini

Department of Enterprise Engineering "Mario Lucertini"

University of Rome "Tor Vergata"

Email biancolini@ing.uniroma2.it

Authors:

Ubaldo Cella, Corrado Groth (*University of Rome "Tor Vergata"*)

Elia Daniele, Angelo De Fenza (*3D TECH Engineering*)



Table of Contents

1	Introduction	2
2	Wind tunnel tests requirements	2
3	Test Facility	2
4	Wind Tunnel model design	3
4.1	Structural dimensioning	5
5	Model elements dimensioning	7
5.1	Pressure taps installation	10
5.2	Strain gauges installation	11
	Appendix	13



1 Introduction

The present document details the design of the test article used to validate the numerical methods developed within the RIBES project. A brief introduction describing the background of the model design is first provided. The progress of the development, according to the results of the analysis performed, will be reported together with the description of the final test article configuration.

2 Wind tunnel tests requirements

The purpose of the wind tunnel measurements campaign is to provide an experimental database strongly customized to the validation of the numerical tools developed within the RIBES project. The requirements for the tests and for the WT models are:

- For the tests
 - static pressure and strain measurements under steady flow conditions
 - Forces and moments measurements
 - Model deformation measurements (photogrammetric techniques)
- for the model
 - scaled physical model of a metallic wing type of structure
 - rectangular shape and small thickness
 - installation of strain gauges and pressure pick-up points at its surface

The idea at the base of the proposal was to develop a WT model which was significant for a realistic design problem maintaining the requirements to be experimentally verified in a low speed wind tunnel (in order to contain the costs). Furthermore, the model was supposed to be a test case as most representative as possible of the fluid- structure interaction phenomenon.

3 Test Facility

The reference wind tunnel in which to perform the test is the low speed facility of the university of Naples "Federico II" (Figure 1). The test section is 2 meter wide, the airflow speed limit is 45 m/s and a balances measurement limits are 100Kg for the lift and 20 Kg for the drag. The model will be installed on the side wall of the test section as a cantilever.

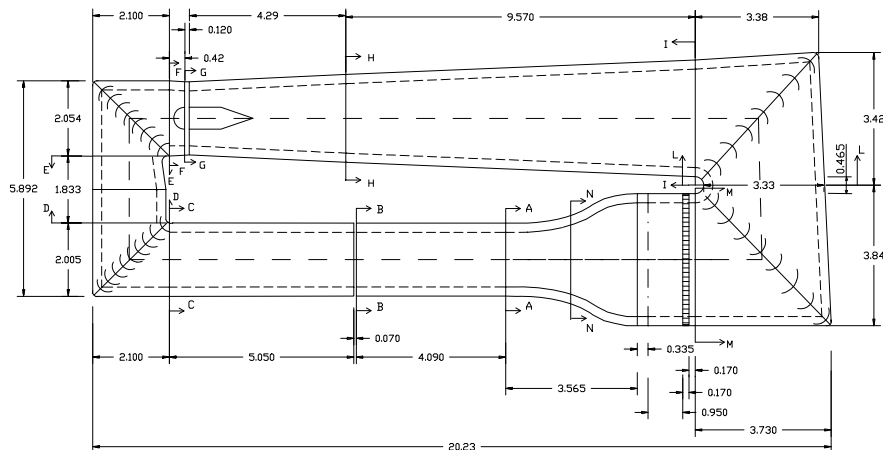


Figure 1: detail of the Naples wind tunnel test facility.

The test matrix is planned to focus the attention around the design lift coefficient and in a range of speed below an over the design speed (ranging from 35 to 45 m/s). Transition trips will be located on both side of the model in order to guarantee a fully turbulent boundary layer and to reduce the risk of separation. The measurement of a free transition polar is however planned.

Lift, drag and pressure coefficient will be measured during all the test matrix runs. Strain gauges measurements and deformation visualization will be reported at the most significant polar points.

4 Wind Tunnel model design

The test case should accomplish the task of being significant for a realistic design problem and of being suitable to be experimentally tested in a low speed wind tunnel. The two objectives are conflicting in several practical aspects. An opportune compromise has then to be selected. The first requirement is accomplished developing a typical wing box structure. The latter is achieved by an opportune aerodynamic design aimed to replicate as much as possible, at wind tunnel conditions, a potential reference aircraft target load distribution. A complete structural and load similitude at testing conditions is, however, impracticable for many reasons. The design compromise consists then in accepting a lower model wing load, respect to a full-scale geometry, maintaining the similitude in the shape of the surface load distribution.

The test article design had a long development process in which several iterations, with the model manufacturer and the topic manager of the project, led to reconsider the original wing configuration proposal. The first topology was thought with the vision to include an aero-structural coupling by adopting a sweep angle and to design a wing suitable for a reference realistic aircraft. A complete structural and load similitude at testing conditions of a scaled wing, however, would have required a relatively high speed which is not compatible with a typical not pressurized low speed wind tunnel with a sufficient large test section. Furthermore, a simple scaling of a “real wing” is not feasible for manufacturing reasons (the thickness of the skin would reduce to impracticable dimensions). A design, expressly customized for our purpose, had then to

be planned. The aerodynamic design of the wing was made selecting an opportune geometric twist and designing a new airfoil specifically with the objective to reproduce as much as possible, at wind tunnel conditions, the pressure distribution the reference aircraft would exhibit in cruise. The complexities encountered related mainly in the attempt to maximize the wing deformation (in order to facilitate the displacement visualization) maintaining the wing box topology and constraining the sheet metal thickness to dimensions that allow a safe model assembly by rivets. Preliminary analyses of candidate dimensioning confirmed the difficulties in obtaining a tip displacement, under a maximum measurable loads (by wind tunnel balances) in the order of 100 kilograms of lift, higher that 1% of the wing span. It was then decided to release the requirement of referring to a realistic aircraft (in order to orient the design only on the measurements requirements without constraints), to eliminate the sweep angle (in order to focus on the structural verification aspect of the FSI mechanism without interferences of other effects) and to comply the manufacturer suggestion to simplify the model geometry (in order to reduce costs and risks of manufacturing uncertainty).

Among the configurations that were designed and verified aerodynamically and structurally, a straight wing 1.6 meters wide, with a root chord of 600 millimetres and 0.7 as taper ratio, was selected as final configuration (Figure 2). In order to simplify its manufacturing, no twist was adopted. The skin is simply obtained by lofting a single curvature surface between the root and the tip airfoils geometries (the airfoil is maintained unchanged along all span).

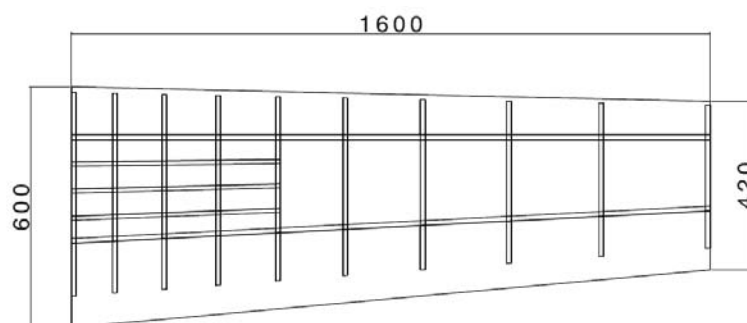


Figure 2: layout of RIBES wing and planform dimensions.

The airfoil was designed starting from the *Göttingen 398* scaling the original shape to a thickness $t/c = 11\%$ and redesigning the leading edge in order to improve the stall performance. Figure 3 reports the designed wing section.

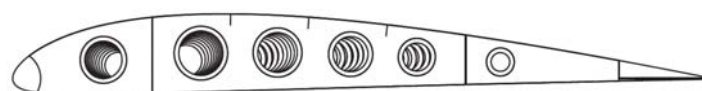


Figure 3: airfoil of the wing.

4.1 Structural dimensioning

The wing box is a typical aeronautical structure with two C-shaped spars and ten ribs. The front spar is located at 20% of the chord and is maintained orthogonal to the symmetry plane. A moderate negative sweep angle (in the order of -0.3 deg.), referred to the line passing through the 25% of the chords, is then present. The rear spar is located at 65% of the chord. The reference surface is 0.816 m². The external skin is divided in four parts: an upper, a lower a leading edge and a V-shaped trailing edge panel. They are joined to the structure by flush head CherryMAX rivets. The model is connected to the wind tunnel balance by a flange and a tubular rod (Figure 4). The wing components were subjected to two treatment before assembly. The first was an Alodine treatment to prevent corrosion while the second consisted in a primer to prepare the wing structure to paint.

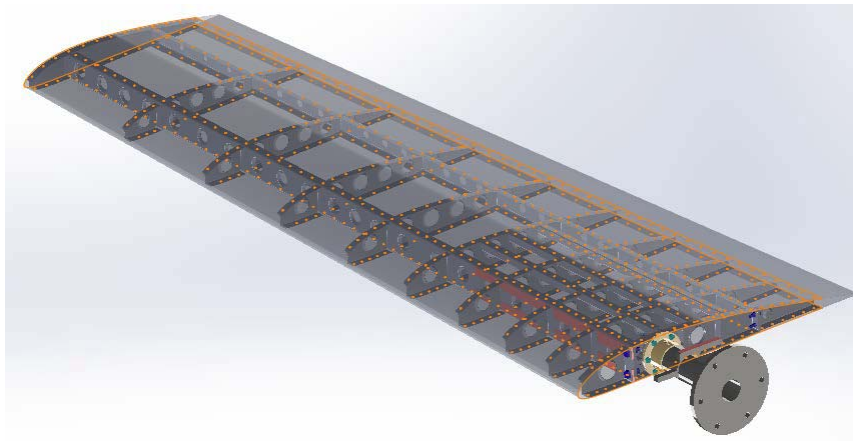


Figure 4: wing model assembly.

The model was dimensioned verifying the design at the target operative condition: flow speed equal to 40 m/s and around 60 kilograms of lift force. The CFD domain used in this phase reproduced the test section, including the inlet convergence element, of the selected wind tunnel facility (Figure 5).

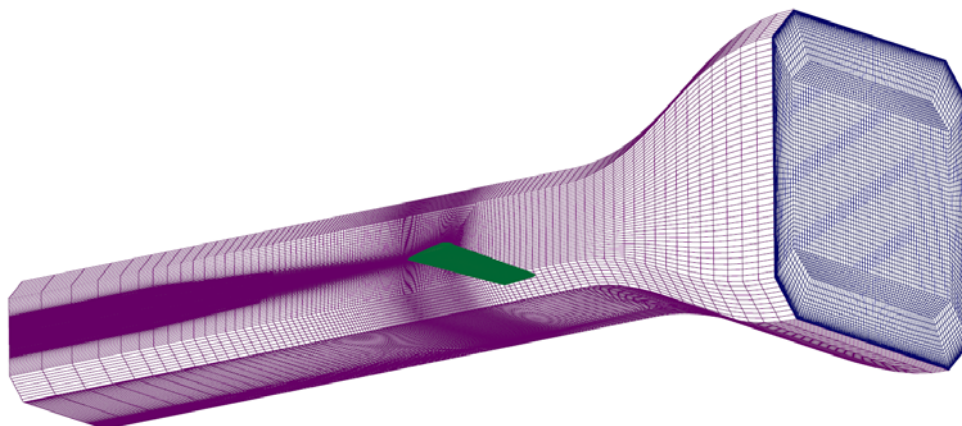


Figure 5: wind tunnel CFD domain.

The mesh was composed by 3.5 million of hexahedral elements. The boundary layer was solved up to the wall of the wing model while wall functions were applied to the tunnel walls. In Figure 6 the obtained spanwise load distribution (left) and the shape of pressure distribution on the wing surface (right) is reported. The load is enough close to the target spanwise elliptical distribution. In this condition, 60 kilograms of lift is generated with a lift coefficient equal to 0.74.

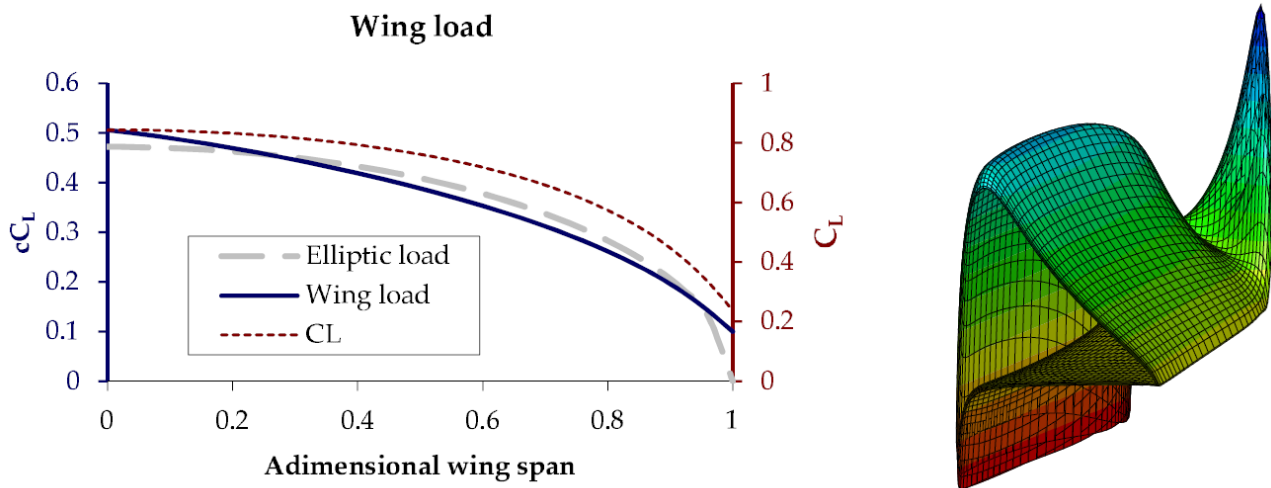


Figure 6: aerodynamic load on the wing surface.

The FEM analysis was essential to dimension the thickness of the sheet metal components and to reinforce the regions of stresses concentration. It was, furthermore, adopted to check the plates buckling onset. This aspect was, in fact, the main driver in dimensioning the model. In order to maximize the wing deformation, the target thickness of spars and skin should be minimized. With this configuration most of the load is carried out by the skin. The buckling verification identified instability problems on the upper skin in the root region where plates are subjected to maximum compression.

The maximum stress observed in design conditions is lower than 40MPa which is very far from the limits of the material (the adopted material is the 2024-T3 aluminium alloy which has a yield strength higher than 270 MPa). From this point of view, the RIBES model dimensioning followed an unusual philosophy. Aircraft wings design, in fact, is typically oriented on weight saving adopting the minimum Factors of Safety, on the primary structures, required by airworthiness authorities (in some case it is considered acceptable the structure to operate with plates in post-buckling conditions). The RIBES wing had as main target the maximization of the deformability of the structure which oriented its dimensioning toward the minimization of the plates thickness (both spars and skin) up to the minimum values acceptable for elements assembly.

Another important observation is that if the load is supported mainly by the skin, plates buckling would cause the whole load to be transferred suddenly to the spars which, if not properly dimensioned, might not be able to sustain the load. Thickening the spars, on the other hand,

would increase the stiffness of the model further reducing the already moderate deformation (the maximum tip displacement computed never exceeded 10 millimetres even reducing the safety margins to one). Although aircraft industries usually assume a safety margin equal to one (or even lower) at limit loads when dimensioning plates for buckling, the final strategy adopted for the RIBES wing was to approach the design in a conservative way thickening the spars and assuming a safety factor between 1.2 and 1.3 on maximum load at buckling onset. With this view, two plates 4 millimetres thick were added in the root region on the front spar where concentrations of stresses were observed.

5 Model elements dimensioning

Two linchpins to link the front spar to the ribs have been used. They are of type “AN” with a diameter of 7.92 mm typical of aeronautical structure. The value of the diameter is due to reduce the bearing for the spar and rib. The two spars thickenings are also aimed to reduce the linchpins loads between rib and spar (Figure 7). The distance between the two linchpins is 40 mm. Knowing the root bending moment, reduced of 20% magnitude in order to take into account the contribution absorbed by rear spar and skin (conservative assumption), the linchpins load is 1527 kg for each one.

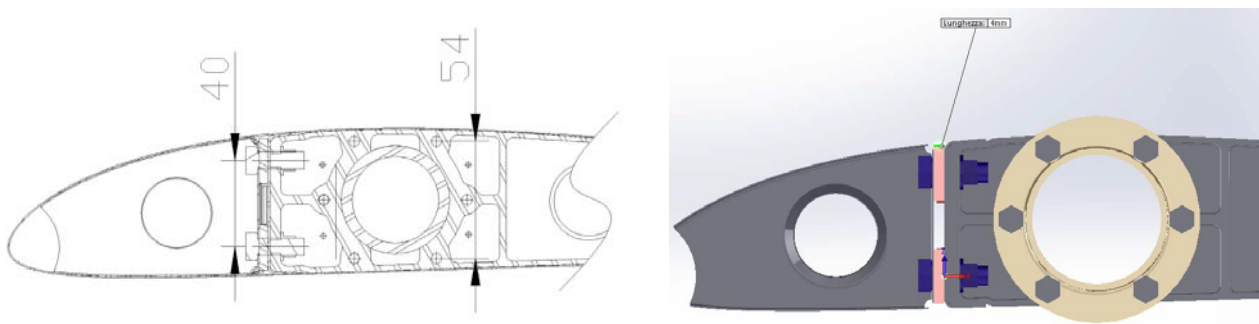


Figure 7: Detail of Linchpins between first rib and front spar

The bearing stress calculation is shown below:

80% bending moment at root:	$M = 61Kg\,m$
Linchpins distance:	$d = 40mm$
Linchpins load:	$F = 1527Kg$
Spar thickening:	$t = 4mm$
Bearing value:	$B = \frac{F}{7.92mm \cdot t} = 48 \frac{Kg}{mm^2}$
Bearing limit:	$B_{lim} = 53 \frac{Kg}{mm^2}$



For the linchpins between first rib and flange, the following assumptions have been made:

- Linchpins of 4.75 mm (traction load)
- Flange contribution neglected (conservative)
- Tubular rod contribution neglected (conservative)
- Distance between top-bottom linchpins equal to 54 mm

The results of calculation are shown below:

100% of bending moment:	$M = 76Kgm$
Top-bottom linchpins:	$d = 54mm$
Number of linchpins collaborating:	$N = 2$
Linchpin load:	$F = \frac{M}{d N} = 703Kg$
Normal limit linchpin 4,75mm:	$F_{lim} = 1288 \frac{Kg}{mm^2}$
Margin:	$+0.54$

The tubular rod, linked between wing model and wind-tunnel structure has to overcome both bending and torsion moment. The following verifications have been made:

- Stress in the flange linked to the wind tunnel structure
- Torsion in the hole zone useful to pass the pressure and strain gauges.

The tubular rod is STEEL material with the following characteristic:

- $\sigma > 400 \frac{N}{mm^2}$
- $\varnothing_{out} = 50mm$
- $\varnothing_{in} = 40mm$
- $t = 5mm$
- $I = 181.132mm^4$

The rod Inertia I has to be verified for a bending moment equal to the maximum wing root bending moment plus the bending moment due to the shear at root times its arm equal to 0.186 m (Figure 8).

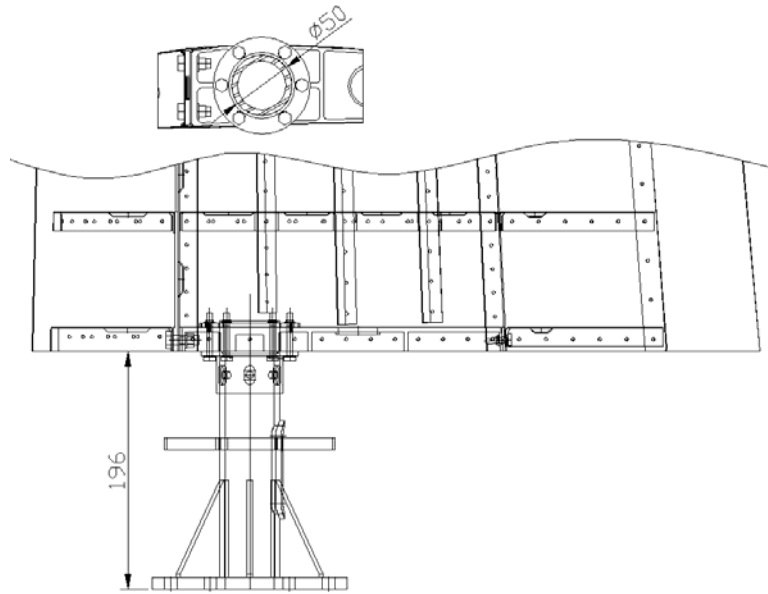


Figure 8: Link between model and wind-tunnel balance

The total bending is equal to:

$$M = M_{aero,max} + T(y = 0) \cdot 0.186m = 96.3kg$$

From this maximum load, the stress is equal to $\sigma = 133 \frac{N}{mm^2}$ with a margin $\gg 1$.

Starting from the torsion maximum moment equal to $M_{tor} = 26Nm$, with Bredt formulas for an open section (the tubular section has a hole for pressure and strain gauges as evidenced in Figure 9), the following results have been obtained:

Maximum torsion moment:	$M_T = 26.000Nmm$
Length of opened section:	$a = 122.8mm$
Thickness:	$t = 5mm$
Tangential stress:	$\tau = \frac{3 M_T}{a t^2} = 25.4 \frac{N}{mm^2}$

Combining the stress due to bending and torsion the Von Mises stress are:

$$\sigma_{v.mises} = \sqrt{\sigma^2 + 4\tau^2} = 143 \frac{N}{mm^2} \ll \sigma_{allowed}$$

This value is far enough from material limit.

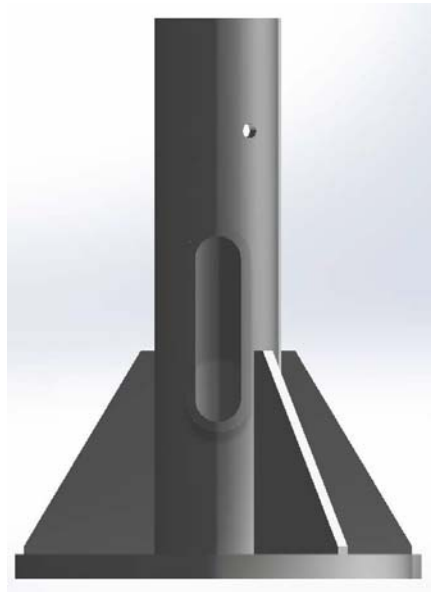


Figure 9: Tubular rod and flange for the link to the WT balance

5.1 Pressure taps installation

A number of 80 pressure taps have been installed in 6 sections of the model (Table 1 and Figure 10). Section 1, 2, 4 and 6 are instrumented with only 4 pressure taps each one on the upper surface, in order to check pressure distribution. Section 3 and Section 5 are instrumented with 38 and 26 pressure taps in order to evaluate pressure distribution and wing span loading

Table 1: Pressure taps locations and number

Section	Y [mm]	η	Chord [mm]	n. pressure taps
1	160	0.1	582	4
2	450	0.281	549	4
3	600	0.375	533	38
4	1000	0.625	488	4
5	1200	0.75	465	26
6	1600	0.938	431	4
				Total 80

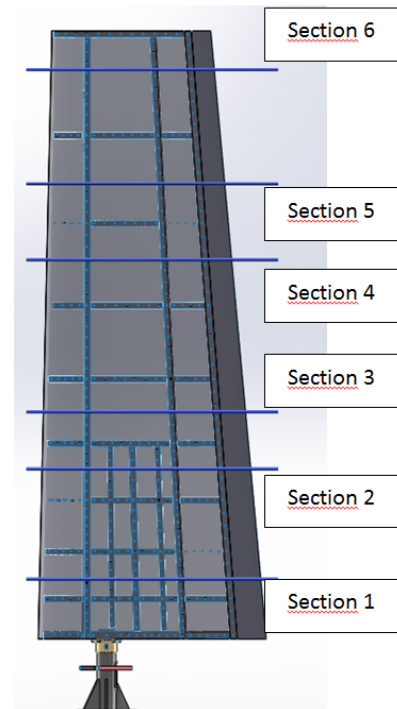


Figure 10: Pressure taps sections

Eighty Pressure taps tubes will be linked to the wing model skin and then wired into the model and carried outside the model through the tubular rod hole. Pressure taps installation and wiring satisfies the following items:

- Tubes outer diameter is 2 mm
- Tubes inner diameter is 1 mm
- Tubes do not coincide with rivets and ribs
- Tubes go through ribs and spars holes
- Minimum pressure taps distance > 4mm

5.2 Strain gauges installation

Twenty-five (16 unidirectional plus 3 rosette with 3 signals) strain gauges have been installed on the wing model, as summarized in Table 2 and Figure 11.

Table 2: Strain gauges locations number, number and type

ID	Bay	POSITION	INSTALLATION	TYPE	y (mm)
1	1	between rib1-rib2	front spar	UNIDIRECTIONAL	35.5
2	1	between rib1-rib2	front spar	UNIDIRECTIONAL	35.5
3	1	between rib1-rib2	rear spar	UNIDIRECTIONAL	35.5
4	1	between rib1-rib2	rear spar	UNIDIRECTIONAL	35.5
5	3	between rib3-rib4	front spar	UNIDIRECTIONAL	310
6	3	between rib3-rib4	front spar	UNIDIRECTIONAL	310
7	3	between rib3-rib4	rear spar	UNIDIRECTIONAL	297
8	3	between rib3-rib4	rear spar	UNIDIRECTIONAL	297
9	5	between rib5-rib6	front spar	UNIDIRECTIONAL	600
10	5	between rib5-rib6	front spar	UNIDIRECTIONAL	600
11	5	between rib5-rib6	rear spar	UNIDIRECTIONAL	598
12	5	between rib5-rib6	rear spar	UNIDIRECTIONAL	598
13	1	between rib1-rib2	front spar thickening	UNIDIRECTIONAL	35.5
14	1	between rib1-rib2	front spar thickening	UNIDIRECTIONAL	35.5
15	1	1stbay, between 1st and 2nd stringer	Upper Skin	UNIDIRECTIONAL	35.5
16	1	1stbay, between 2nd and 3rd stringer	Lower Skin	ROSETTE-3SIGNAL	35.5
17	2	2ndbay, between 1st and 2nd stringer	Upper Skin	UNIDIRECTIONAL	169
18	2	2ndbay, between 2nd and 3rd stringer	Upper Skin	ROSETTE-3SIGNAL	169
19	1	between rib1-rib2	front spar	ROSETTE-3SIGNAL	35.5

The strain gauges aim to provide the following measurements:

- Strain gauges from 1 to 12 (unidirectional) located on the front and rear spar caps provide information on how bending moment is differently absorbed by the spars, along spanwise (3 different wing sections).
- Strain gauges 13 and 14 (unidirectional) give information on the efficiency of increased stiffness provided by the thickening of the front spar.
- Rosette 19 (0°-45°-90° directions) allows measuring the complete state of strain of the shear web, including possible diagonal tension state.
- Strain gauges and rosettes from 15 to 18 (unidirectional), placed on the upper (unidirectional 15, 17 and rosette 18) and lower (rosette 16) wing skin, monitor tension (compression, traction) levels and eventual panel instability occurring close to the wing root.

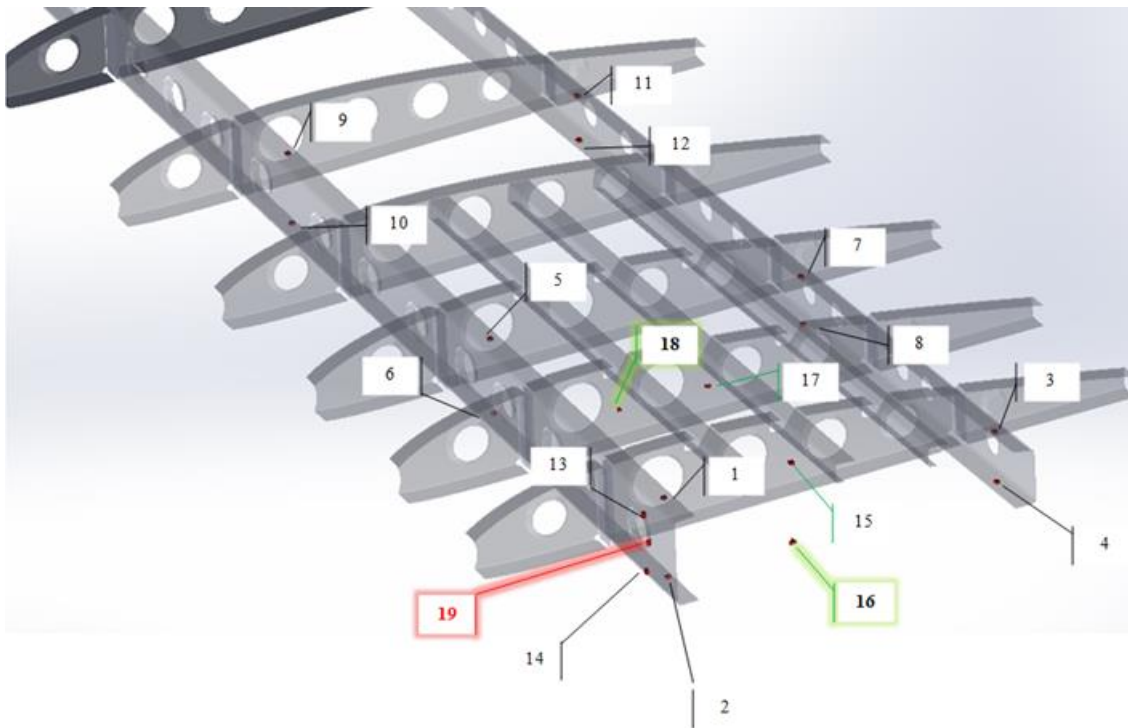


Figure 11: Strain gauges installation

Appendix

List of wing elements

- n.1 front spar (thickness 1 mm, thickening between 1st and 4th bay) (Section 4.1)
- n.1 rear spar (thickness 1 mm) (Section 4.1)
- n.2 front spar thickening (Section 4.1)
- n.9 wing box ribs (thickness 0.6 mm) (Section 4.2)
- n.9 leading edge ribs (thickness 0.6 mm) (Section 4.2)
- n.9 trailing edge ribs (thickness 0.6 mm) (Section 4.2)
- n. 3 stringers on the upper surface (thickness 0.6 mm) (Section 4.3)
- n.1 skin upper box (thickness 0.6 mm) (Section 4.4)
- n.1 skin lower box (thickness 0.6 mm) (Section 4.4)
- n.1 skin leading edge (thickness 0.6 mm) (Section 4.4)
- n.1 skin V shaped for the trailing edge (thickness 0.4 mm) (Section 4.4)

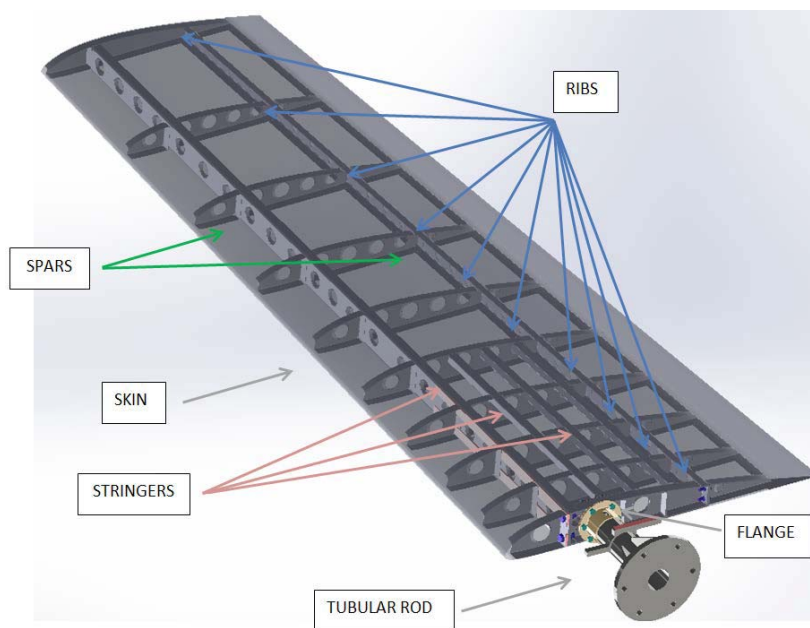


Figure 12: Wing components

Junctions elements

- n. 800 (eight hundred) rivets cherry max (see Section 4.4 and 4.5)
- n.6 (six) linchpins of 4.8 mm AN type
- n.6 (six) nuts of 4.8 mm MS210442 or equivalent type
- n.2 (two) linchpins of 7.92 mm e n.2 (two) nuts to join front spar to the 1st ribs.
- n.2 (two) linchpins of 4.8 mm e n.2 (two) nuts to join rear spar to the 1st ribs.

Spars



Figure 13: Spars and root rib

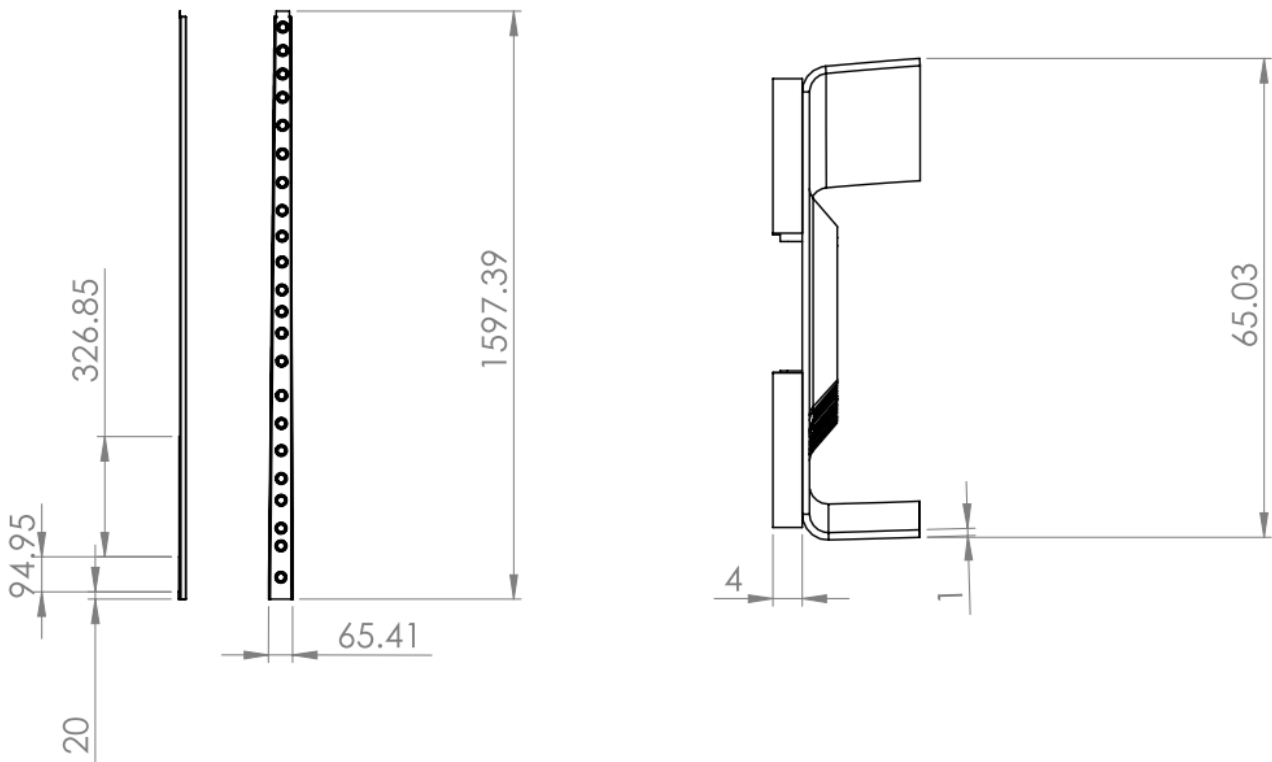


Figure 14: Front spar dimensions

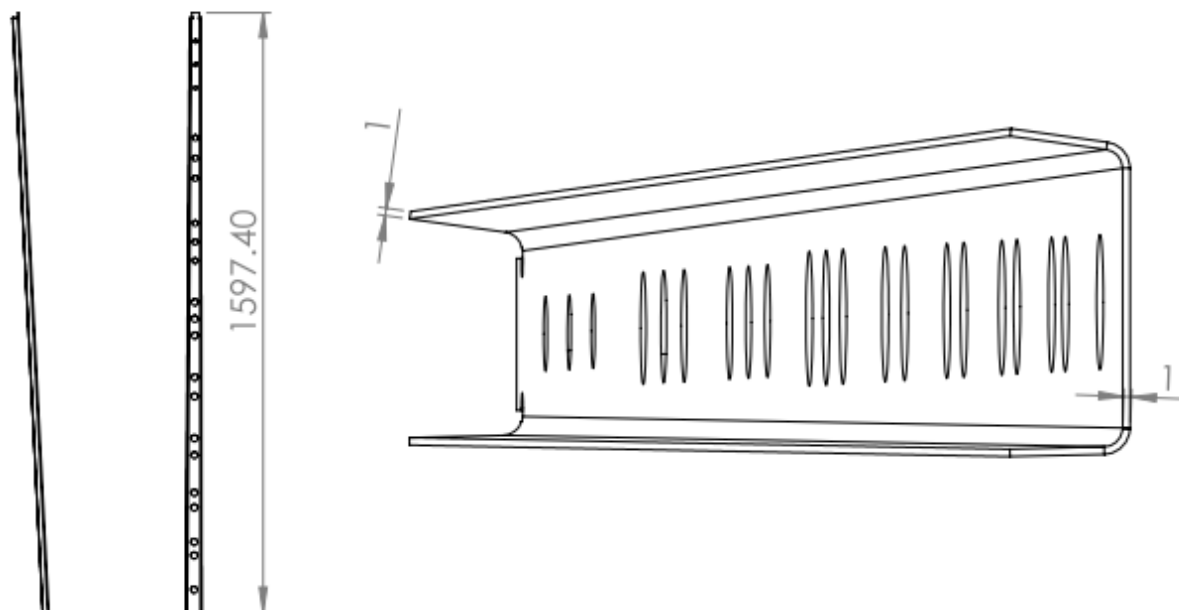


Figure 15: Rear spar dimensions

Ribs

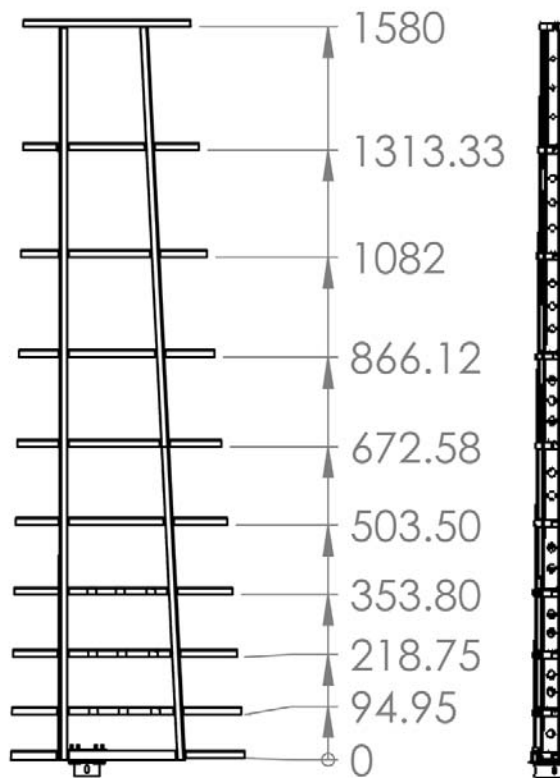


Figure 16: Ribs spacing

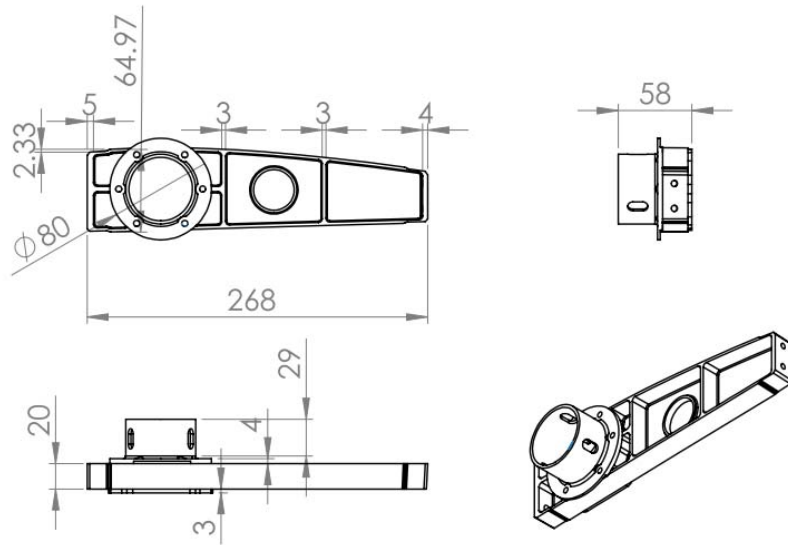
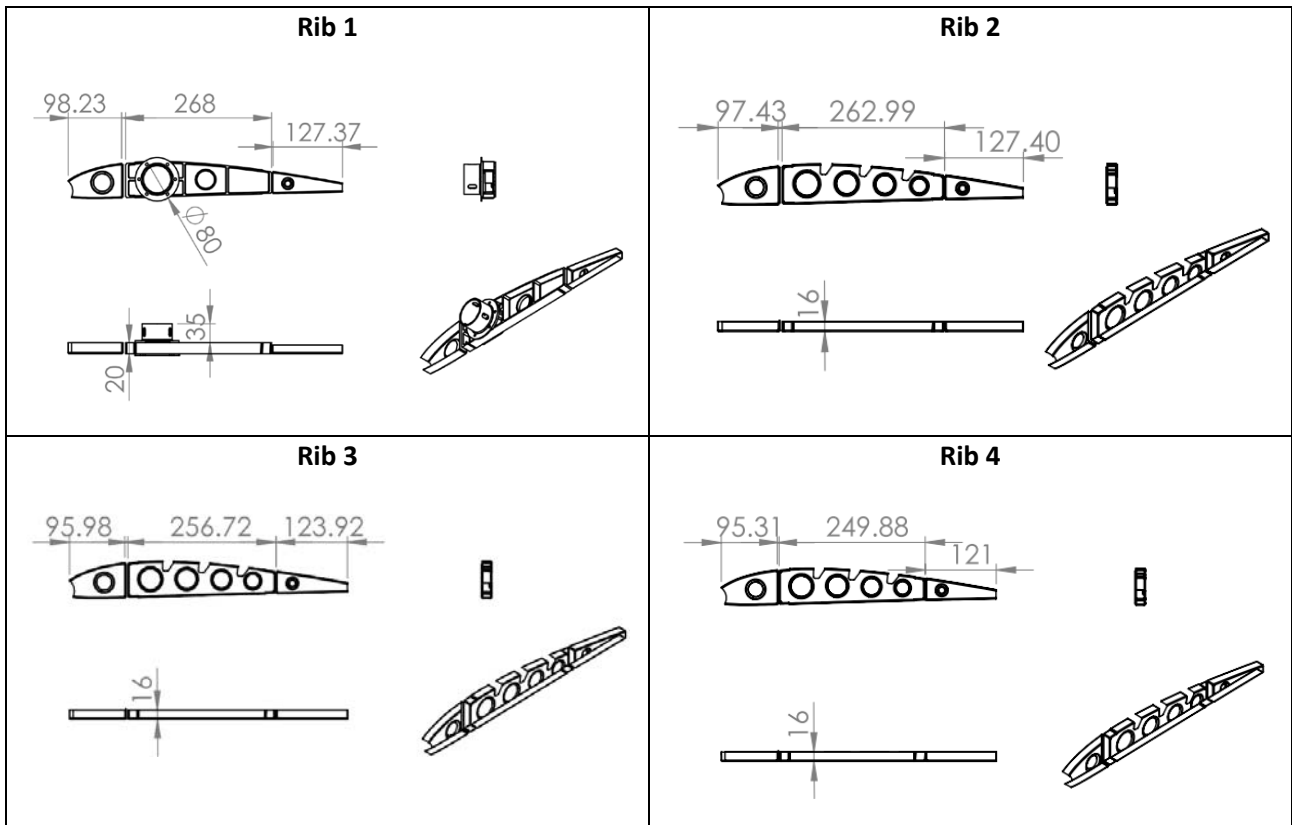


Figure 17: Root rib dimensions



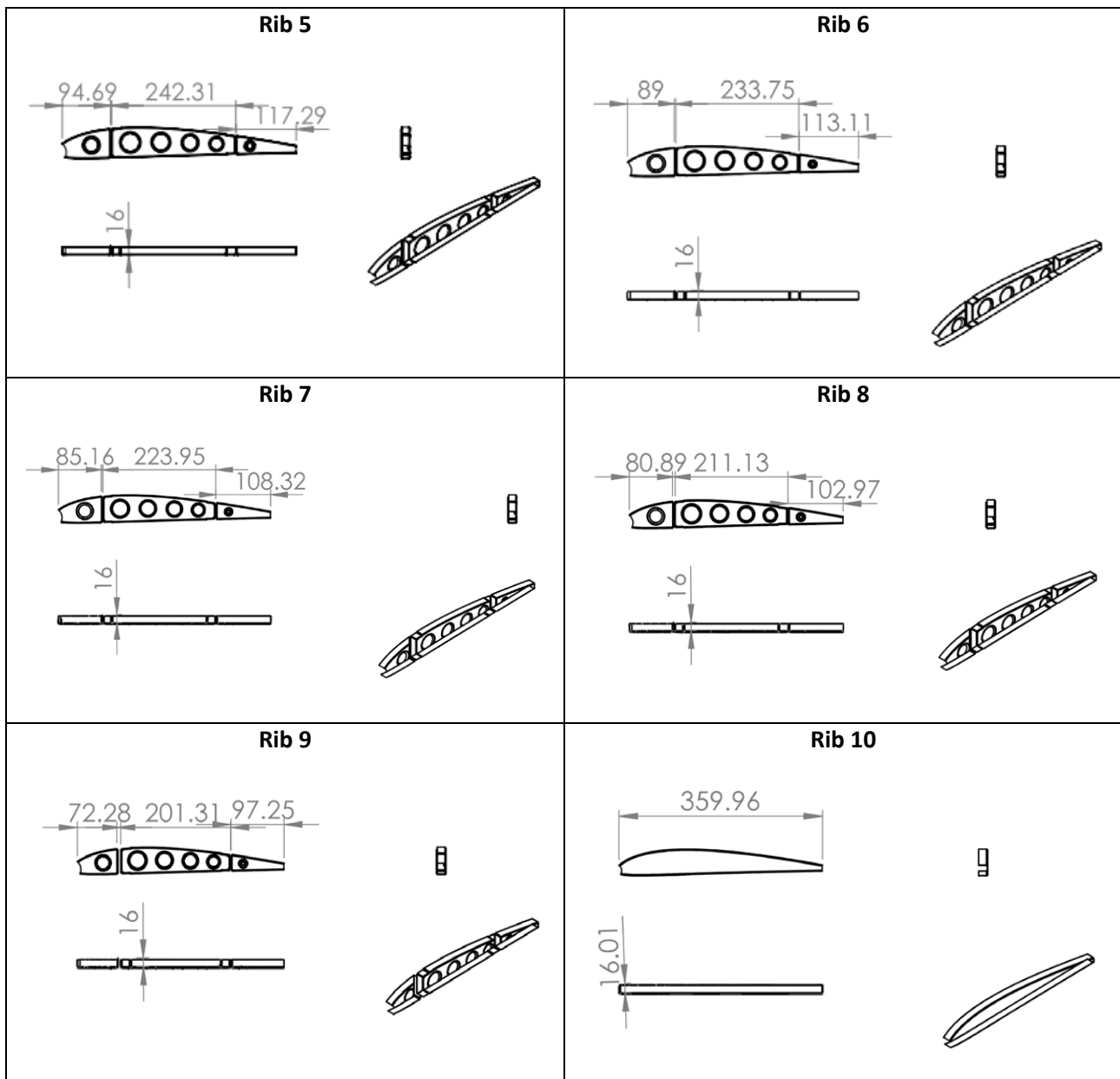


Figure 18: Ribs dimensions

Stringers

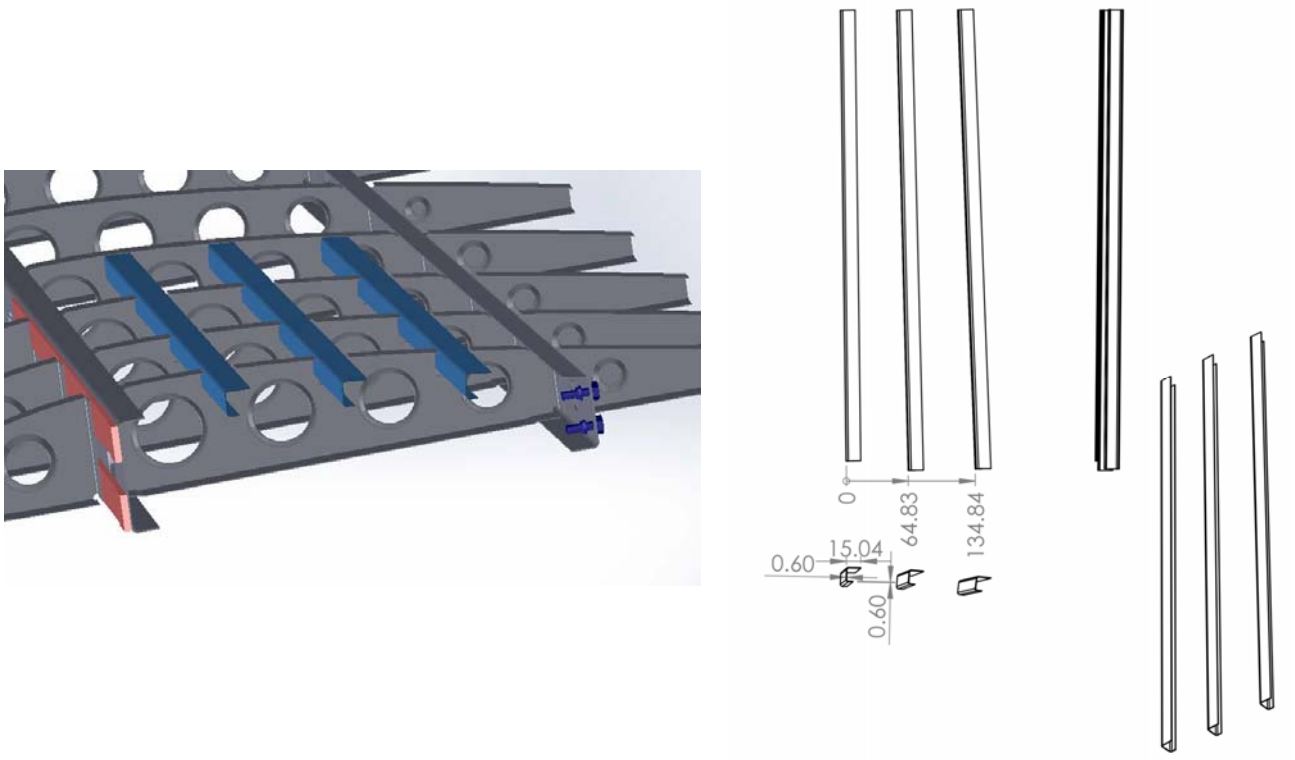


Figure 19: Stringers dimensions

Skin

The skin is divided into 4 components: upper panel, lower panel, leading edge and trailing edge. The thickness of all of them is 0.6 mm with the exception of the trailing edge V skin which is 0.4 mm.



Figure 20: Skin panels

Flange and tubular rod

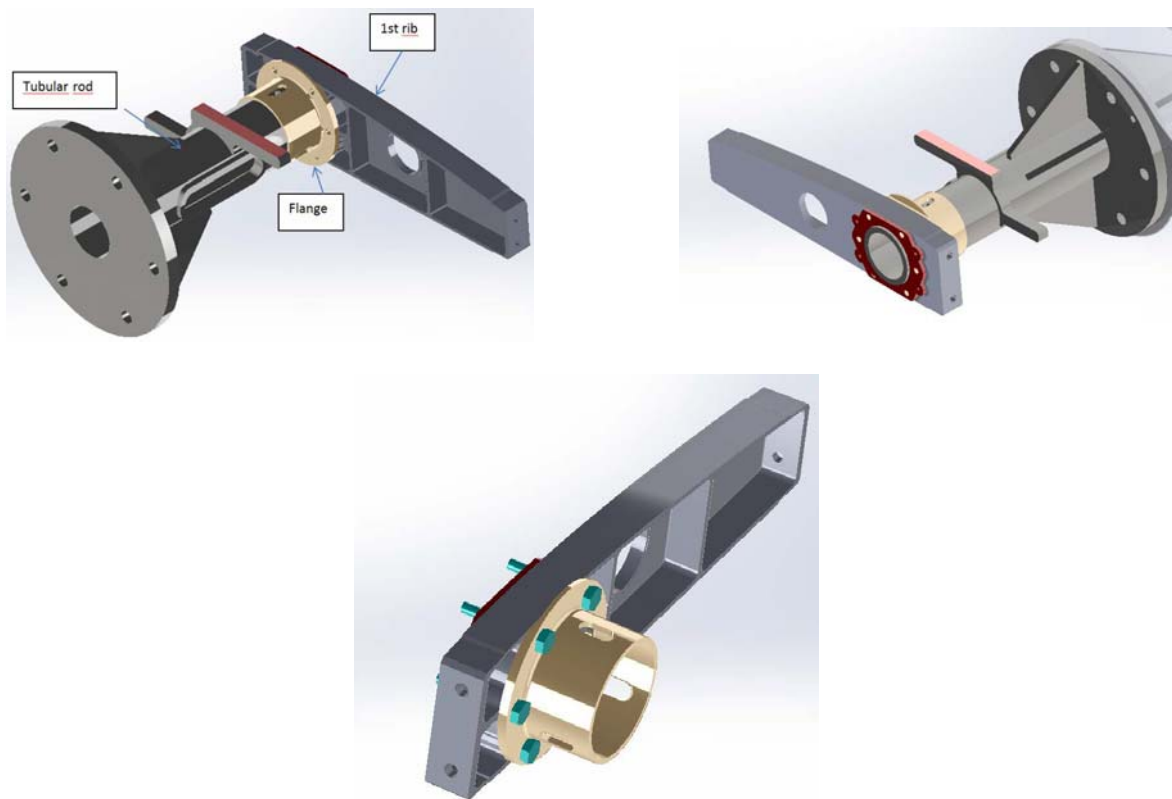


Figure 21: Details of flange and tubular rod

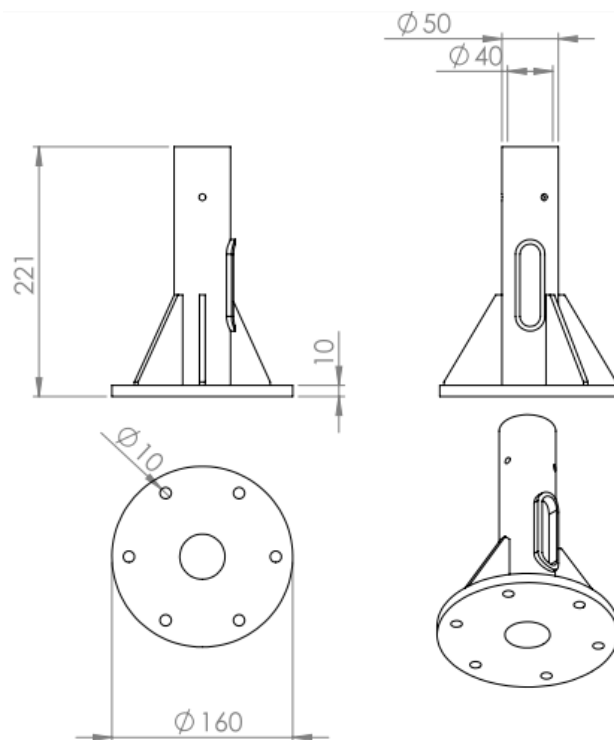


Figure 22: Tubular rod dimension